

Hoop-Passing Motion for a Snake Robot to Realize Motion Transition Across Different Environments

Tatsuya Takemori^{ID}, Student Member, IEEE, Motoyasu Tanaka^{ID}, Member, IEEE,
and Fumitoshi Matsuno^{ID}, Member, IEEE

Abstract—A snake robot performs diverse motions. To realize a wide range functions in a complex environment, it is necessary to transition between various motions suited to each environment. In this article, we propose a method of transitioning the motion of a snake robot across different environments to expand the application environment of the robot. We first find that the motion at the connection point between two motions must coincide with the tangential movement during motion transition across different environments. We then design a gait called the circular pedal wave. This circular pedal wave allows a hoop-passing motion in which the whole body moves as if it is passing through a virtual hoop fixed in space in sequence from its head through combination with a proposed shift part. The hoop-passing motion allows motion transition across different environments. We propose three application examples of this hoop-passing motion, namely passing through a hole in a wall, entering an underfloor, and attaching to a ladder. We report on experiments conducted to verify the effectiveness of the proposed method and to realize the described motions.

Index Terms—Biologically-inspired robots, redundant robots, search and rescue robots, snake robot.

I. INTRODUCTION

BIOLOGICAL snakes, despite having simple and limbless bodies, adapt to various environments through a variety of behaviors; e.g., when moving over uneven terrain and climbing trees. A snake can also grasp an object by wrapping itself around it. A snake robot, which is based on a biological-snake mechanism, is expected to solve a variety of problems while having a simple structure, and much research has been done on relevant control methods [1]. A control method that converges the controlled quantity to a target value using a model has been proposed. Two main models are used for this method:

Manuscript received November 24, 2020; accepted February 24, 2021. Date of publication March 26, 2021; date of current version October 1, 2021. This work was supported by the ImPACT Program of the Council for Science, Technology, and Innovation (Cabinet Office Government of Japan). This article was recommended for publication by Associate Editor M. Rubenstein and Editor M. Yim upon evaluation of the reviewers' comments. (*Corresponding author: Tatsuya Takemori*.)

Tatsuya Takemori and Fumitoshi Matsuno are with the Department of Mechanical Engineering and Science, Graduate School of Engineering, Kyoto University, Kyoto 606-8501, Japan (e-mail: takemori.tatsuya.23a@st.kyoto-u.ac.jp; matsuno@me.kyoto-u.ac.jp).

Motoyasu Tanaka is with the Department of Mechanical and Intelligent Systems Engineering, The University of Electro-Communications, Tokyo 182-8585, Japan (e-mail: mtanaka@uec.ac.jp).

This article has supplementary material provided by the authors and color versions of one or more figures available at <https://doi.org/10.1109/TRO.2021.3063438>.

Digital Object Identifier 10.1109/TRO.2021.3063438

a friction model that does not take nonholonomic constraints into account [2]–[4] and a model that does take nonholonomic constraints into account [5]–[11]. Such a method using a model of interaction between the robot and environment is effective for simple environments such as those on a plane.

In a complex environment with obstacles that are difficult to model, methods of propulsion using obstacles in a manner similar to that adopted by a biological snake has also been studied [12]–[15], which called “obstacle-aided locomotion”.

There is another approach in complex environments to realize locomotion, which design the overall form of the snake robot. Although such an approach does not involve kinematic or kinetic optimization, it is easy to apply to complex environments that cannot be modeled. A variety of gaits, such as *sidewinding* and *lateral rolling*, can be realized by directly defining the trajectory of the joint angle of the snake robot as a parameterized equation [16]–[19]. However, when the target form of a snake robot becomes more complex, it is difficult to directly formulate a joint angle trajectory that realizes that form.

Without using gait functions, the target form is represented by a continuous spatial curve called the *backbone curve* [20], and a method of approximating a discrete snake robot to this curve has been studied [21]–[30]. Adopting this method, a snake robot is abstracted into a continuous curve, and the advantage is that it is easy to design complex forms because the joint angles do not need to be determined directly. We extended the approximation method of Yamada and Hirose [24] and proposed a method of designing the target form of a snake robot by connecting the *curve segment* [31]. In addition, by using our motion design method, we proposed motions that allow the robot to move over a flange on a pipe and a *crawler gait* for moving over uneven ground. Furthermore, we designed a ladder-climbing gait and developed a novel snake robot with a smooth surface shape, and realized ladder climbing with the snake robot [32]. On the basis of these studies [16]–[32], we can design corresponding motions of a robot for propulsion to some specific irregular environments.

The motion of a snake robot is diverse, and the effectiveness of a motion depends on the configuration of the snake robot and environmental conditions. In realizing diverse functions in a complex environment, it is necessary to transition between diverse motions suitable for each environment. Methods adopted for the movement of a snake robot across a discontinuous environment have been studied [33]–[35]. However, these methods are limited in their motion pattern and target environments.

In this article, we take a step towards our ultimate goal developing a unified method for snake robot to transition between environments by transitioning between common snake motions. Now, we focus on the motions commonly used in snake robots and consider a method for transitioning between them across different environments. In Section III, in preparation for the mathematical description of motion, we extend the method of designing target forms by connecting simple shapes and formulate a method of designing new target forms by connecting several target forms. In Section IV, we discuss the motion transition of a snake robot and decide on the realization of a hoop-passing motion as a problem to be solved in this article. In Section V, we propose a method of realizing a hoop-passing motion. In Section VI, we propose application examples of the proposed hoop-passing motion, such as passing a hole in a wall, passing a hole in the floor, and attaching to a ladder from the floor. In Section VII, we verify the effectiveness of the proposed method by conducting experiments with our snake robot developed in [32]. Finally, Section VIII concludes this article.

II. RELATED WORK

This section describes the details of the related work mentioned in Section I.

A. Obstacle-Aided Locomotion

Liljebäck *et al.* [13] realized efficient obstacle-aided locomotion adopting compliance control that fits the obstacle on the side directed toward where the snake robot wants to proceed but does not fit the obstacle on the opposite side. Kamegawa *et al.* [14] introduced motion based on a serpenoid curve that is a reflexive behavior for obstacle contact. Kano *et al.* [15] realized autonomous and decentralized promotion with obstacles by feeding back reaction forces received from the environment. These studies considered a plane with obstacles as an environment.

B. Motion Design With Continuous Curve

In [20]–[24], methods of obtaining the joint angles to approximate the robot to the backbone curve were proposed. Andersson [21] proposed a method of matching the joint positions from the beginning to the target curve in a multilinked robot connected with universal joints. However, when each joint has only one degree of freedom, it is not possible in principle to match all the joint positions to the curve, and the approach is not applicable. Hatton *et al.* [22], therefore, proposed annealed chain fitting, which approximates the target curve from the beginning by minimizing the evaluation function corresponding to the magnitude of the distance between the target curve and robot. Liljebäck *et al.* [23] proposed a method of approximating the snake robot to a curve drawn by connecting the *shape control points* in a three-dimensional (3-D) space. Yamada and Hirose modeled a snake robot using Frennet–Serret’s formula in [25] and proposed a method of deriving appropriate joint angles based on the curvature and torsion of the target curve in [24].

The approximation method of Yamada and Hirose [24] has the advantage that it can be easily applied when the curvature and torsion of the target form are easy to determine, and it has been applied in many studies [27]–[30]. In these studies, the target joint angles were calculated using the method of Yamada and Hirose [24] from the curvature and torsion calculated from the target continuous curve representing the target form. However, it is difficult to represent an appropriate continuous curve analytically when a more complex target form is required. Additionally, the target joint angle cannot be calculated using the method of Yamada and Hirose [25] because of the divergence of the torsion if there is a region where the curvature is zero on the curve. We, therefore, extended the method of Yamada and Hirose [24] and proposed a method of designing the target form of a snake robot by connecting the *curve segment* whose properties, such as curvature and torsion, are already known [31].

C. Locomotion Across Discontinuous Environments

Several methods for the movement of a snake robot across a discontinuous environment have been proposed. Fu and Li [33] developed a snake robot with compliant passive wheels that can move from one horizontal plane to another after overcoming a step. Nakajima *et al.* [34] demonstrated that a snake robot with passive wheels can move across nonparallel planes. In these studies, a specific environment was considered and a corresponding movement method was proposed for each environment. This is a limitation of these studies. Kano *et al.* [35] proposed a TEGOTAE-based (“Tegotae” is a Japanese concept that describes how well a perceived reaction matches an expectation) decentralized control scheme for switching behavior in response to changes in the environment, such as those in a parallel-wall or random-obstacle environment. In this method, different locomotion patterns emerge from a single decentralized control rule. However, this method is applicable to only a 2-D plane.

III. GAIT DESIGN AND FITTING METHOD

In this section, we explain the method used to express a target form of a snake robot and approximate the form of the snake robot to the target form, proposed in [31].

A. Shape Fitting Using the Backbone Curve

We use a snake robot model that is comprised of alternately connected pitch-axis and yaw-axis joints. A previous study [24] showed that this configuration gives the best approximation. The number of joints is represented by n_{joint} and the link length is l . The upper value of the limitation of the absolute angle of a joint is θ_{\max} .

We explain the relationship between the Frenet–Serret frame and the backbone curve and the approximation method, which was proposed in [25] and [24]. The backbone curve is used to express the target form of the snake robot. Let a spatial continuum curve be $c(s)$, where s is the length variable along the curve. As shown in Fig. 1, $e_1(s)$, $e_2(s)$, and $e_3(s)$ are the unit vectors that form the orthonormal basis, which is called the *Frenet–Serret*

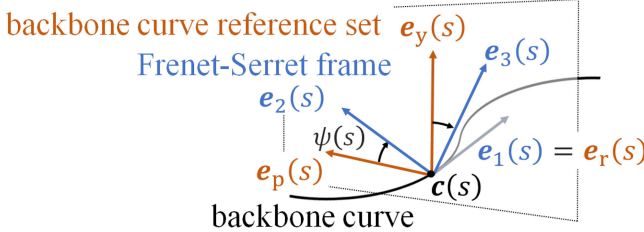


Fig. 1. Difference between the Frenet–Serret frame and the backbone curve reference set [31].

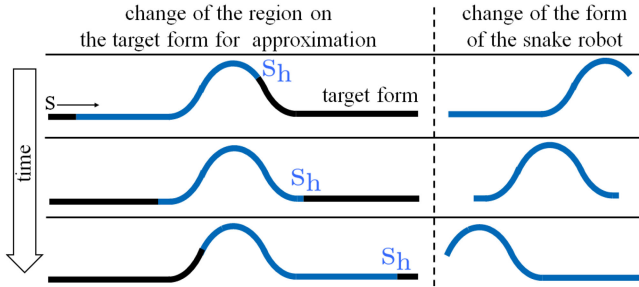


Fig. 2. Concept of shift control.

frame. Curvature $\kappa(s)$ corresponds to the change in the direction of $e_1(s)$ while torsion $\tau(s)$ corresponds to the change in the direction of $e_2(s)$. In contrast with the Frenet–Serret model, the backbone curve reflects the joint direction in the modeling of the snake robot. As shown in Fig. 1, a *backbone curve reference set* comprising $e_r(s)$, $e_p(s)$, and $e_y(s)$ is defined on the curve by considering the snake robot to have the form of a continuous curve. $e_r(s)$ is equal to $e_1(s)$. $e_p(s)$ is a unit vector that is oriented along the pitch axis and $e_y(s)$ is a unit vector that is oriented along the yaw axis. These vectors constitute the basis vectors of the *backbone curve reference set*. As shown in Fig. 1, $\psi(s)$ is the twist angle of the Frenet–Serret frame and the backbone curve reference set around $e_1(s)$, which can be obtained from $\tau(s)$ as

$$\psi(s) = \int_0^s \tau(\hat{s}) d\hat{s} + \psi(0) \quad (1)$$

where $\psi(0)$ is an arbitrary integral constant that corresponds to an initial angle.

We consider the curvature based on the backbone curve reference set. $\kappa_p(s)$ and $\kappa_y(s)$ are, respectively, the curvatures around the pitch axis and yaw axis in the backbone curve reference set and can be obtained as

$$(\kappa_p, \kappa_y) = (-\kappa(s) \sin \psi(s), \kappa(s) \cos \psi(s)). \quad (2)$$

Finally, the target angle of each joint is calculated using

$$\theta_i^d = \begin{cases} \int_{s_h-(i-1)l}^{s_h-(i+1)l} \kappa_p(s) ds & (i : \text{odd}) \\ \int_{s_h-(i-1)l}^{s_h-(i+1)l} \kappa_y(s) ds & (i : \text{even}) \end{cases} \quad (3)$$

where s_h is the head position of the snake robot on the target continuous curve.

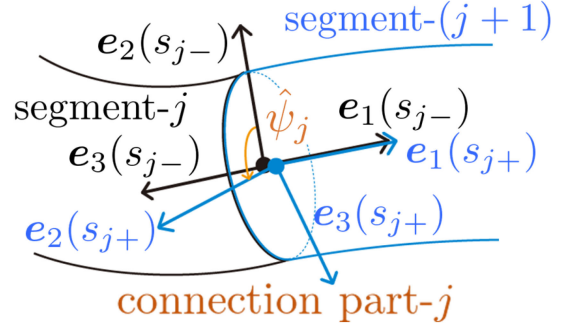


Fig. 3. Joint between segments [31].

As shown in Fig. 2, by changing s_h smoothly, the corresponding region on the target form to the approximated form of the snake robot changes, then the snake robot can change its form smoothly. This control method is called *shift control*. The basic concept of shift control is described in [1]. This shift control method based on backbone curve can generate motion without directing motion in joint space. Shift control is used to generate various motion such as wave like motion, sliding motion, peeling motion. In addition to that, it can be used in various ways, for example when there is an obstacle or when the snake robot has wheels.

B. Backbone Curve Connecting Simple Shapes

It is difficult to represent complex target forms analytically. There is also the problem that the torsion may sometimes become infinite if there are regions of zero curvature within the target form [25]. To solve these problems, we proposed a method of expressing the target form based on the connection of simple shapes for which the curvature and torsion are clear [31]. Using this method, we can design the target form intuitively. The simple shapes that are connected in this method are called *segments*. This section describes how the target form can be configured by connecting these segments; this replaces the first step of the shape fitting process.

At the *connection part*, in which segments are connected, the Frenet–Serret frame is discontinuous. It is, therefore, necessary to devise a representation of the target form. When counting from the tail side, the j th segment is referred to as *segment j* ($j \in \mathbb{N}$). $s = s_j$ is the point of connection part j , which connects segment j and segment $(j+1)$, and is obtained from the length of segment j l_j

$$s_j = s_{j-1} + l_j \quad (4)$$

where $s_0 = 0$ is the beginning point of the target form of the snake robot.

The state of connection part j is shown in Fig. 3. s_{j-} and s_{j+} are, respectively, the points at infinitesimal distances before and after connection part j . The Frenet–Serret frame, curvature, and torsion at s_j are represented by corresponding values at s_j .

The curvature and torsion of segment j are, respectively, denoted κ_j and τ_j . The curvature of the target form $\kappa(s)$ and

the torsion $\tau(s)$ are obtained as

$$(\kappa(s), \tau(s)) = (\kappa_j, \tau_j) \quad (s_{j-1} < s \leq s_j). \quad (5)$$

We next consider the twist at the connection part. As shown in Fig. 3, the angle between $e_2(s_{j-})$ and $e_2(s_{j+})$ around $e_1(s_{j-})$ is denoted $\hat{\psi}_j$. To consider this twist angle within the relationship between the Frenet–Serret frame and the backbone curve, (1) must be replaced by

$$\psi(s) = \int_0^s \tau(\hat{s}) d\hat{s} + \psi(0) + \sum_j \hat{\psi}_j u(s - s_j) \quad (6)$$

where $u(s)$ is the step function. The first step of the shape fitting procedure is now replaced and the desired joint angles of the snake robot can thus be obtained using (2) and (3) based on (5) and (6). To design the target form, we must first determine the shape of each segment and the twist angle $\hat{\psi}_j$.

In this article, we use a straight line and a circular arc as simple shapes of segments in which the curvature and torsion are constant. In the case of a straight line, the Frenet–Serret frame and torsion are not defined. In this article, we newly define torsion to be zero so that the straight-line segments can be handled in the same way as other segments. The frame inside the straight line is defined as being equal to the frame at $s = s_{j-}$ and the torsion is zero. A circular arc, in which the curvature is constant and the torsion is zero, is defined by its radius r_j and its central angle ϕ_j . The length of a circular arc segment is calculated to be $r_j \phi_j$.

IV. PROBLEM SETTING

A. Appropriate Motion at the Boundary

Let us consider an environment E_i and a corresponding motion M_i in E_i . We define B_{ij} as a boundary surface between E_i and E_j and define NB_{i-j} (NB_{j-i}) as a neighborhood of B_{ij} inside E_i (E_j). As a snake robot should move across the boundary of a connected environment of E_i and E_j with discontinuity, our problem is to design a connection motion between two different movements M_i and M_j of the robot in E_i and E_j . At the boundary B_{ij} , the velocity vector of the motion of the robot inside E_i should coincide with that inside E_j during the transition. This is a boundary condition. In general, it is difficult for M_i to coincide with M_j at B_{ij} . We propose connection motions CM_{i-j} and CM_{j-i} in NB_{i-j} and NB_{j-i} , which satisfy the boundary condition, to connect motions M_i and M_j that the robot can move across from E_i to E_j . The definitions are shown in Fig. 4. In Fig. 4, CP_{ij} is the connecting point between the part for CM_{i-j} and the part for CM_{j-i} in the snake robot.

In the transition process, we consider which motion of CM_{i-j} and CM_{j-i} at B_{ij} meets the boundary condition. Let the length of the part for CM_{j-i} and M_j in the snake robot at time t be $L_{j-i}(t)$, as shown in Fig. 4. In this article, we simplify the problem by assuming the following movement across B_{ij} .

- 1) The snake robot moves in E_i and approaches B_{ij} ($L_{j-i} = 0$).
- 2) The head of the snake crosses B_{ij} and enters NB_{j-i} and E_j with L_{j-1} increasing from 0 (at the moment the head

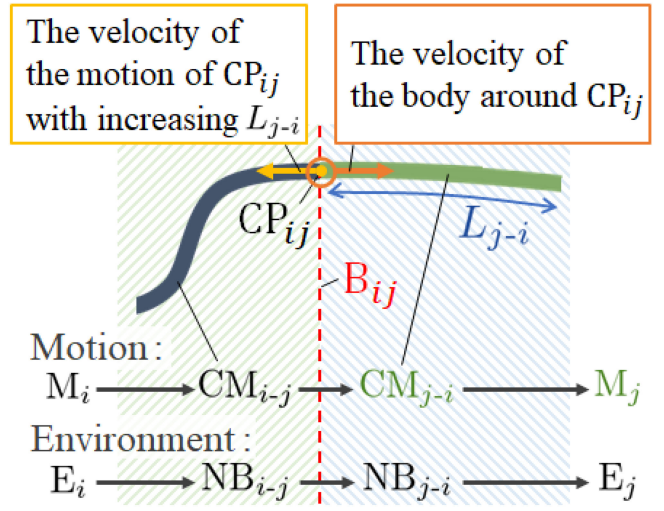


Fig. 4. Schematic diagram of motion transition.

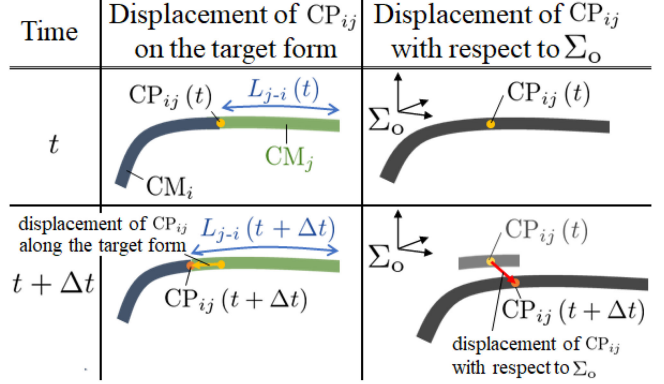


Fig. 5. Displacement of CP_{ij} .

reaches B_{ij}) to L_{robot} , once the whole robot has entered NB_{j-i} and/or E_j .

Therefore, from the beginning to the end of the motion transition from CM_{i-j} to CM_{j-i} , L_{j-i} varies from zero to the full length of the snake robot. Let us consider the displacement from $CP_{ij}(t)$ to $CP_{ij}(t + \Delta t)$, as shown in Fig. 5. $CP_{ij}(t)$ is a point at a length $L_{j-i}(t)$ from the beginning of the CM_{j-i} side of the snake robot at time t . Boundary conditions (BC1 and BC2) that ensure the velocities of CM_{i-j} and CM_{j-i} at CP_{ij} match in the tangential direction of the trunk to cancel out the motion of CP_{ij} resulting from changing L_{j-i} are expressed as follows.

BC 1: CP_{ij} must move along the tangential direction of the curve of the snake robot form while changing $L_{j-i}(t)$.

BC 2: CP_{ij} does not move at the environmental boundary B_{ij} with respect to the inertial coordinate system Σ_o (w.r.t Σ_o) during motion transition, which means that the displacement between $CP_{ij}(t)$ and $CP_{ij}(t + \Delta t)$ must be zero.

In such a transition process, the snake robot passes through only one point in the boundary surface B_{ij} (the position of $CP_{ij}(t)$ is invariant). This means that we do not have to take

TABLE I
CLASSIFICATION OF MOTION TRANSITION

M_i (Motion in E_i)	CM_{i-j} (Motion in NB_{i-j})	CM_{j-i} (Motion in NB_{j-i})	M_j (Motion in E_j)
TP	-	-	TP
TP	-	?	Non-TP
Non-TP	?	-	TP
Non-TP	?	?	Non-TP

into account the complexity of the shape of the boundary surface B_{ij} , simplifying the transition motion.

B. Classification of Motion Transition

In many motions of snake robots, the whole body slips in the tangential direction of each part. Taking the example of the snake robot that is constrained in the normal direction of the trunk by its passive wheels [5]–[11] or obstacles [13]–[15], the constrained part of the body moves in the tangential direction of the trunk. In the case of the ladder-climbing gait [32], although there is no constraint in the direction parallel to the steps of the ladder, the whole body of the robot moves in a tangential direction. We then classify motions such that the movement of the point of connection with other motion can be kept in a direction tangential of the trunk during a motion transition as *tangential propulsion* (TP) type motion. This means that TP-type motion satisfies BC1 and BC2 without any special connection motion CM_{i-j} and CM_{j-i} between TP-type motions during a transition.

Meanwhile, there are many motions that are not of TP-type, which are classified as non-TP-type motions. Examples of such motions are sidewinding [36], the 3-D pedal wave [37], and the crawler gait [31], which are motions in which the point of contact between the robot and environment does not move spatially. These motions are important because they can be adopted even when slippage between the robot and environment is not allowed owing to, for example, high friction with the environment. Additionally, the propulsion does not require frictional anisotropy and is, thus, effective when a snake robot without passive wheels moves in a nonobstacle environment. The nonwheeled snake robot with no anisotropy of friction has the advantage that it can be fabricated with a simple configuration and is easy to make waterproof and dustproof by attaching a cover. Additionally, an operation that adopts rolling, such as helical rolling [27], [28], [30], which can move inside and outside the pipe, is an example of non-TP-type motion. Thus, depending on the configuration of the snake robot and environment, there are many cases in which non-TP-type motions are required. However, in such motions, it is difficult to meet the boundary conditions in performing motion transition.

As the motions of snake robots are classified into TP-type and non-TP-type motions in this article, we have two possibilities for the motion M_i (M_j) in the environment E_i (E_j). We can classify motion transition into four cases $(CM_{i-j}, CM_{j-i}) \in \{\text{TP-type, Non-TP-type}\} \times \{\text{TP-type, Non-TP-type}\}$, as shown in Table I. Note that TP-type motion does not require connection motion and can be directly connected because TP-type motion

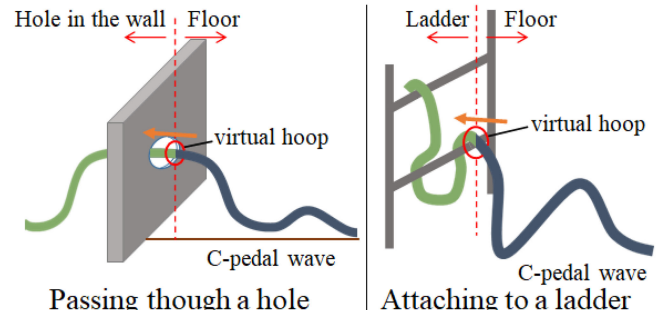


Fig. 6. Application examples of hoop-passing motion.

meets both BC1 and BC2 by definition. Therefore, our problem is to design a connection motion (CM_{j-i} , CM_{j-i}) that satisfies boundary conditions BC1 and BC2 in the case that either or both of M_i and M_j are of non-TP-type.

C. Overview of Hoop-Passing Motion

The abovementioned discussion reveals the importance of proposing a connection motion to achieve motion transition, even in the situation that the snake robot does not slide in the tangential direction of the trunk. In this situation, TP-type motions are not applicable and only non-TP-type motions are available. We refer to motion in which the body is pushed (BC1) and the snake robot passes through a virtual hoop fixed w.r.t Σ_0 (BC2) from head to tail without slippage between the robot and environment as *hoop-passing motion*. The virtual hoop should be fixed at the position, where CP_{ij} should pass on B_{ij} . The plane that includes the virtual hoop should be in contact with the surface of B_{ij} . In this article, a special gait called the *circular pedal wave* (c-pedal wave) is designed to realize the hoop-passing motion. The c-pedal wave is a propulsion motion that does not require passive wheels, obstacles, or frictional anisotropy and does not require slippage between the robot and environment. It is classified as a non-TP-type motion. Additionally, the c-pedal wave can be combined with the newly proposed *shift part* and TP-type motion can be adopted as the connection motion for motion transition. Therefore, the hoop-passing motion, which is detailed in Section V, can be applied as a connection motion in the transition to various motions. Application examples of hoop-passing motion, such as passing through a narrow space or attaching to a ladder, are shown in Fig. 6.

V. HOOP-PASSING MOTION

In this section, the hoop-passing motion is proposed as the connection motion of motion transition for non-TP-type motion. We propose a new gait referred to as the *circular pedal wave*, which is a non-TP-type motion. The C-pedal wave has a form such that wave-shaped units are connected. A feature of the c-pedal wave is that the tangential direction at both ends of the unit is parallel to the direction of propulsion. Additionally, we design a *shift part* to be combined with the c-pedal wave such to push the snake robot head out. It is then possible to execute repeatedly a deforming motion as the snake robot pushes its body

out while satisfying BC1 and BC2. Satisfying BC1 and BC2 is equivalent to passing a point fixed on the boundary surface of the environment with the trunk of the robot parallel to the normal of the boundary surface. This is as if the robot were passing through a virtual hoop fixed in space from its head to tail. The shift part connects the c-pedal wave to the virtual hoop and is the key to realizing the hoop-passing motion.

In the following, we first formulate a method of designing a new target form by connecting multiple target forms. Next, to realize the hoop-passing motion, we describe the design of the c-pedal wave, the design of the shift part, and the execution of the hoop-passing motion. Finally, we introduce the lift part as a typical example of a form that is often used in applications of hoop-passing motion.

A. Form Design by Connecting Forms

We extend the method of representing a target form by connecting curve segments and explain the method of representing a new target form $C(s)$ by connecting several different target forms. The form is obtained in (2) and (3) by determining the curvature $\kappa(s)$ and torsional angle $\psi(s)$.

The number of forms connected is N , and we let the k th form from the beginning be form- k ($k = 1, 2, \dots, N$). Let the curvature and torsion angle of form- k be $\kappa_{fk}(s)$ and $\psi_{fk}(s)$, respectively. The position of the connection part between form- k and form- $k+1$ in $C(s)$ is denoted S_k , and the discontinuous torsion angle at this connection part is denoted $\hat{\Psi}_k$ in the same way as in Fig. 3. Furthermore, $\hat{\Psi}_0$ is determined as the initial torsion angle at $C(0)$.

A schematic diagram of connecting multiple target forms is shown in Fig. 7. Fig. 7 shows an example of $N = 3$. Let s_{fk} be the starting point of the part of form- k to be used for the new target form, and l_{fk} be the length of the part to be used for the new form. The starting point of the new connected form is defined as $S_0 = 0$, and the position of the connected part of each original form has the relationship

$$S_k = \sum_{k=1}^k l_{fk}. \quad (7)$$

Then, the curvature $K(s)$ and torsion angle $\Psi(s)$ in ($S_{k-1} < s \leq S_k$) of $C(s)$ are determined as

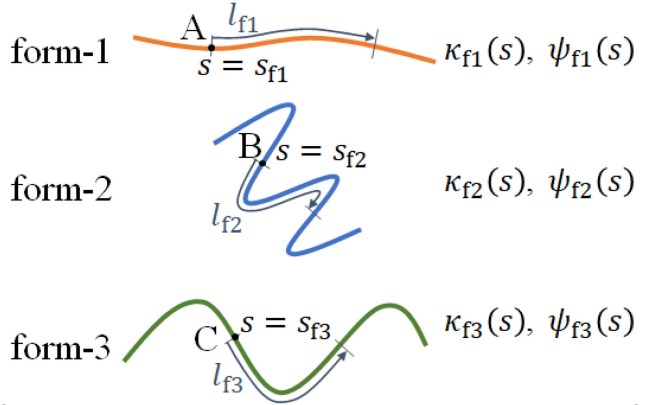
$$K(s) = \kappa_{fk}(s - S_{k-1} + s_{fk}) \quad (8)$$

$$\begin{aligned} \Psi(s) &= \Psi(S_{k-1}) + \hat{\Psi}_{k-1} \\ &\quad + \psi_{fk}(s - S_{k-1} + s_{fk}) - \psi_{fk}(s_{fk}) \end{aligned} \quad (9)$$

here, $\Psi(S_{k-1})$ is the torsion angle of the end of the previous form in the connected form, $\hat{\Psi}_{k-1}$ is the discontinuous torsion angle between form- $(k-1)$ and form- k in the connected form and determined by the motion designer, and $\psi_{fk}(s - S_{k-1} + s_{fk}) - \psi_{fk}(s_{fk})$ is the change of the torsion angle from the starting point on the original form- k .

By determining the form of each original curve to be connected and the torsion angle $\hat{\Psi}_k$ of the connecting part, we can approximate the form of the snake robot from (2) and (3).

【 Original forms 】



【 Connected form 】

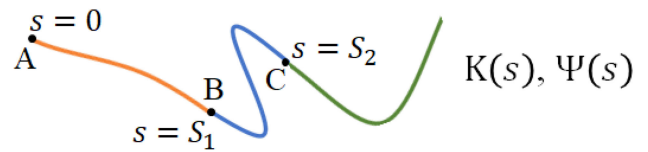


Fig. 7. Diagram of connecting next forms.

TABLE II
PARAMETERS OF SEGMENTS COMPOSING THE CIRCULAR PEDAL WAVE

seg no. j	type	parameter	$\hat{\Psi}_j$
$3n + 1$	arc	$(r_j, \phi_j) = (r_p, \beta_p)$	$(-1)^n \alpha_p$
$3n + 2$	arc	$(r_j, \phi_j) = (r_p, 2\beta_p)$	π
$3n + 3$	arc	$(r_j, \phi_j) = (r_p, \beta_p)$	π

B. Design of Hoop-Passing Motion

The hoop-passing motion is realized by combining a newly proposed gait called the circular pedal wave and a form called the shift part. The end part of the shift part is in the virtual hoop, and the deformation of the shift part pushes the body out through the virtual hoop in a tangential direction. We will explain each form and the motion design.

1) *Circular Pedal Wave*: We propose a new gait called the *circular pedal wave* (c-pedal wave) in the hoop-passing motion. The c-pedal wave is a modification of the 3-D pedal wave proposed in [37] and does not require slippage between the body and environment. At the same time, by combining with the shift part, which will be explained later, it has the property of enabling the hoop-passing motion as TP-type. The c-pedal wave is designed by connecting circular arcs and has the form shown in Fig. 8. The three arcs make a *c-pedal unit*, and the target form is configured by connecting the isomorphic c-pedal units. The form is determined by three gait parameters: the height h_p , width w_p , and wave interval d_p . The shape parameters of each arc that compose the c-pedal wave are given in Table II. The quantity n in Table II is the index of the c-pedal unit. The form of the c-pedal wave projected on the yz plane and the plane parallel to the unit are schematically represented in Fig. 9. Fig. 9 shows that

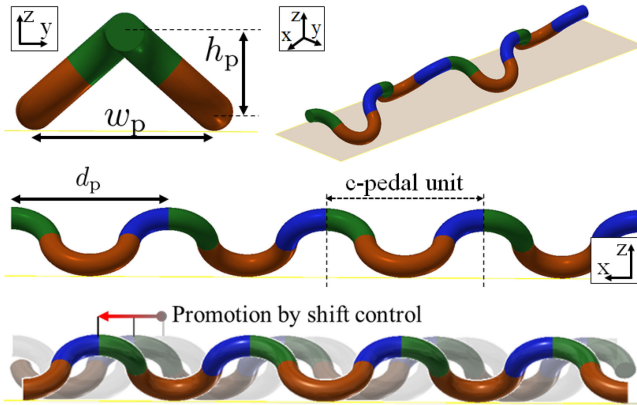


Fig. 8. Overview of circular pedal wave.

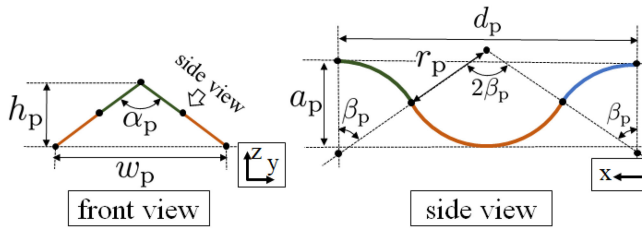


Fig. 9. Diagram of the circular pedal wave.

the radius r_p of all arcs, the angles α_p and β_p , and the lengths h_p , w_p , and d_p in Table II have the geometrical relationships

$$\alpha_p = 2 \arctan \left(\frac{w_p}{2h_p} \right) \quad (10)$$

$$a_p = 2r_p (1 - \cos \beta_p) \quad (11)$$

$$a_p = \sqrt{h_p^2 + \left(\frac{w_p}{2} \right)^2} \quad (12)$$

$$d_p = 4r_p \sin \beta_p. \quad (13)$$

Solving (11) and (13) for r_p and β_p yields

$$r_p = \frac{4a_p^2 + d_p^2}{16a_p} \quad (14)$$

$$\beta_p = 2 \arctan \left(\frac{d_p}{4r_p - 2a_p} \right). \quad (15)$$

According to the abovementioned, once the gait parameters h_p , w_p , and d_p are determined, all other parameters can be obtained using (12), (14), and (15). Additionally, the length of one c-pedal unit l_{pu} is derived as

$$l_{pu} = 4r_p \beta_p. \quad (16)$$

In the case of the c-pedal wave, shift control generates movement in the x -axis direction in Fig. 8 and movement in the y -axis direction can be achieved by a rolling motion. To realize hoop-passing motion that meets BC1 and BC2, the tangents at the two ends of each c-pedal unit are designed to align in a straight

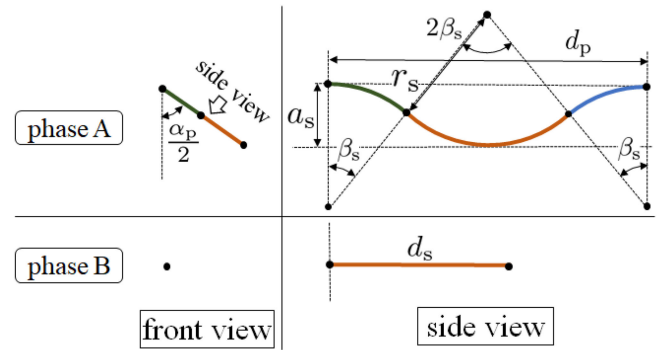


Fig. 10. Forms of the shift part corresponding to operations in phases A and B.

TABLE III
PARAMETERS OF SEGMENTS COMPOSING THE SHIFT PART IN PHASE A

seg no.	type	parameter	$\hat{\psi}_j$
1	arc	$(r_1, \phi_1) = (r_s, \beta_s)$	$\pi + (-1)^{k_r} \alpha_p / 2$
2	arc	$(r_2, \phi_2) = (r_s, 2\beta_s)$	π
3	arc	$(r_3, \phi_3) = (r_s, \beta_s)$	π

TABLE IV
PARAMETERS OF SEGMENTS COMPRISING THE SHIFT CONNECTING PART IN PHASE B

seg no.	type	parameter	$\hat{\psi}_j$
1	straight	$l_1 = d_s$	$\pi + (-1)^{k_r} \alpha_p / 2$

line, and the tangent direction is designed to be parallel to the direction of movement by the shift control.

2) *Shift Part*: The shift part has two segment configurations, corresponding to two operation phases, phase A and phase B. The shift part is transformed by repeating the phase-A operation and phase-B operation alternately. Let the deformation from the initial state of phase A to the end state of phase B be one period and the number of repetitions of this period be k_r . A form of the shift part for each phase is shown in Fig. 10. Additionally, parameters of each segment in phase A and phase B are, respectively, presented in Table III and Table IV. Let the progress of each operation phase be q ($0 \leq q \leq 1$). $q = 0$ means the initial state of the phase and $q = 1$ the end state of the phase.

In phase A, the form of the shift part is determined by the value of a_s , which corresponds to the height of the wave. When $a_s = a_p$, namely $q = 0$, the form of the shift part is the same as that of the c-pedal unit. The value corresponding to the wave interval is fixed at d_p , which is the same value as for the c-pedal wave. From a_s and d_p , $r_s(q)$ and $\beta_s(q)$ are derived using the same computation as for (14) and (15). As the phase progresses, the form parameters change as

$$a_s(q) = (1 - q)a_p + q\epsilon_s \quad (17)$$

where ϵ_s is a minute positive constant that prevents the radius from diverging by the form being a straight line. The form of the shift part coincides with the form of the c-pedal unit when $q = 0$ and becomes almost straight when $q = 1$.

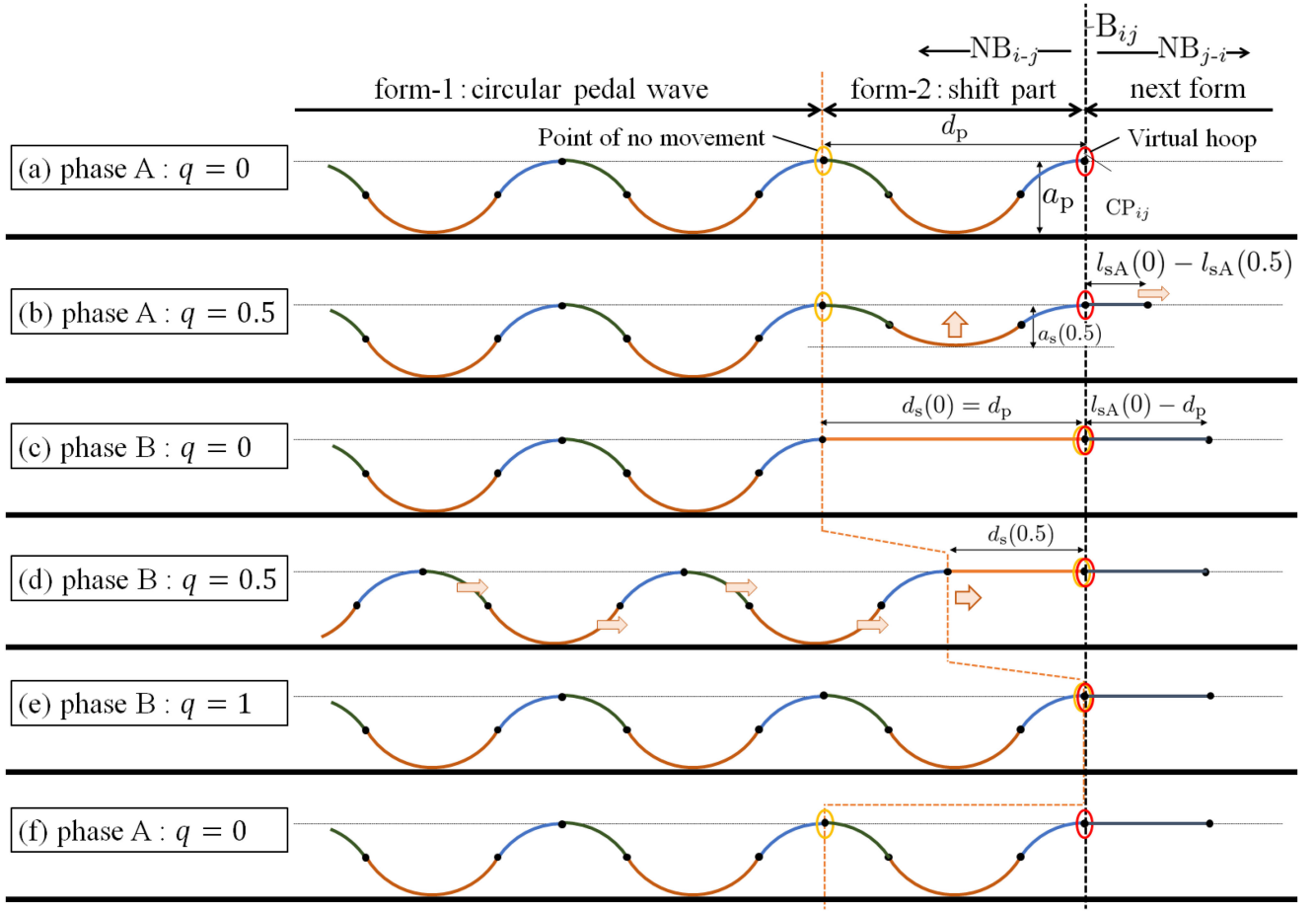


Fig. 11. Process of the hoop-passing motion.

The length $l_{sA}(q)$ of the shift part in phase A is obtained using

$$l_{sA}(q) = 4r_s(q)\beta_s(q). \quad (18)$$

In phase B, the shift part is a straight line and its length $d_s(q)$ is determined to change in length to zero smoothly as

$$d_s(q) = (1 - q)d_p. \quad (19)$$

The length $l_{sB}(q)$ of the shift part in phase B is obtained using

$$l_{sB}(q) = d_s(q). \quad (20)$$

3) Process of the Hoop-Passing Motion: The form of the part beyond the virtual hoop is called the *next form*. We design a transition from the c-pedal wave to the next form by connecting the c-pedal wave, the shift part, and the next form and repeating phase A and phase B. In the method of connecting target forms described in Section V-A, form-1 is the c-pedal wave, form-2 is the shift part, and form-3 and later are the next forms.

The process of the hoop-passing motion is shown in Fig. 11. First, the deformation of phase A [see Fig. 11(a) and (b)] is performed while the position of the connecting part between the c-pedal wave and the shift part is fixed on the robot (i.e., the point of no movement in Fig. 11). This transformation reduces the length of the shift part and increases the length of the next form, and the total length of the shift part and next form is constant. During this deformation, the tangents at the two ends

of the shift part are kept aligned in a straight line, and BC1 is satisfied. At the same time, this deformation does not produce any horizontal frictional force, and the robot thus does not move. Additionally, the positional relationship between the two ends of the shift part does not change. These results mean that BC2 is satisfied. Afterward, in phase B [see Fig. 11(c)–(e)], the c-pedal wave part moves to the next form and the shift part is shortened. During this phase, the tip of the shift part does not move w.r.t. Σ_o because the length that the shift part shortens is equal to the length that the c-pedal wave part travels. This means BC1 and BC2 are satisfied. In the final state of phase B, the c-pedal unit next to the shift part becomes the new shift part in the initial state of the next phase A [see Fig. 11(f)]. The yellow circles in Fig. 11 indicate a part of the body that does not move w.r.t. Σ_o . By repeating this action until the whole body of the robot becomes the next form, the whole body can be pushed through the virtual hoop.

4) Formulation: We formulate the parameters of each form to realize the process described in Fig. 11. The length l_t of the transitioned next form that changes with the hoop-passing motion is defined by

$$l_t = \begin{cases} \{l_{sA}(0) - l_{sB}(q)\} + k_r \{l_{sA}(0) - d_p\} & (\text{phase A}) \\ ((k_r + 1) \{l_{sA}(0) - l_{sB}(0)\}) & (\text{phase B}) \end{cases}. \quad (21)$$

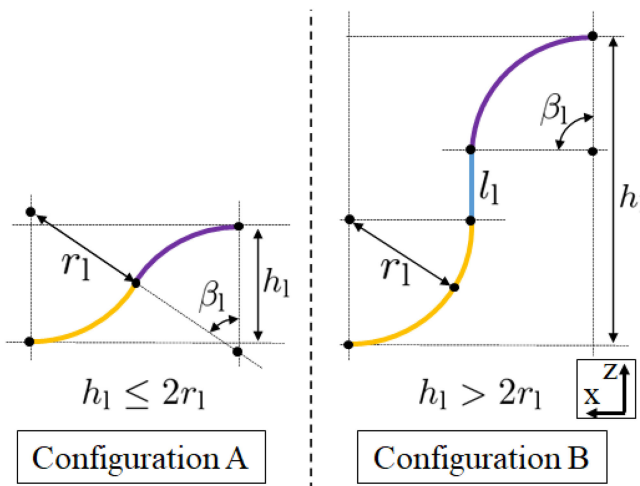


Fig. 12. Configurations of the lift part.

The total length of the snake robot is set to l_{robot} . During the hoop-passing motion, the head position of the snake robot on the target curve is fixed at $s_h = l_{\text{robot}}$, and the lengths l_{f1} and l_{f2} connecting the c-pedal wave and shift part are varied as

$$l_{f1} = \begin{cases} l_{\text{robot}} - l_t - l_{sX} & (l_t + l_{sX} \leq l_{\text{robot}}) \\ 0 & (l_{\text{robot}} < l_t + l_{sX}) \end{cases} \quad (22)$$

$$l_{f2} = \begin{cases} l_{sX} & (l_t \leq l_{\text{robot}}) \\ 0 & (l_{\text{robot}} < l_t) \end{cases} \quad (23)$$

$$l_{sX} = \begin{cases} l_{sA} & (\text{phase A}) \\ l_{sB} & (\text{phase B}) \end{cases}. \quad (24)$$

The length l_{f3} is determined according to the design of the next form. s_{f1} and s_{f2} , the starting points of form-1 and form-2 to be used for the new target form, are specified by

$$s_{f1} = -k_r l_{pu} - l_{f1} \quad (25)$$

$$s_{f2} = 0. \quad (26)$$

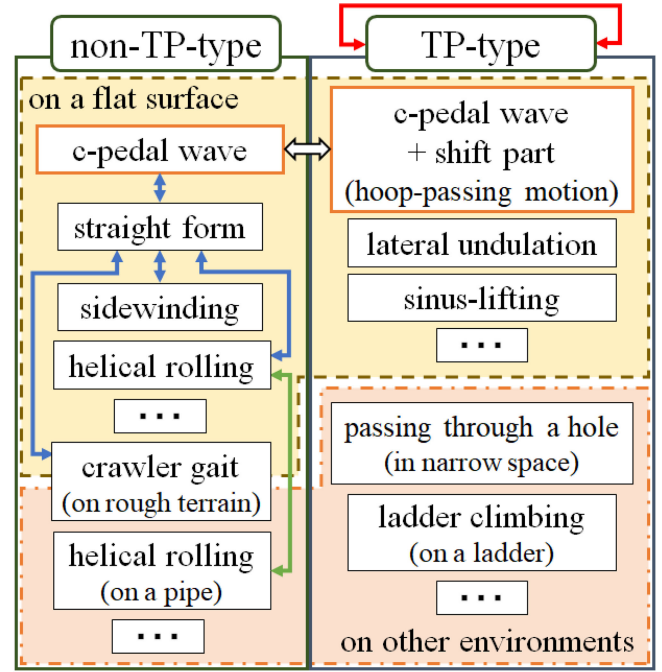
Additionally, the torsion angle $\hat{\Psi}_1$ at the connecting part of the c-pedal wave and shift part is determined using

$$\hat{\Psi}_1 = (-1)^{k_r+1} \alpha_p. \quad (27)$$

C. Lift Part

The next form can be freely designed. We now introduce a typical example of a frequently used form, which is the *lift part*. This form is suitable for lifting the snake robot head further from the position of the virtual hoop. When passing through a hole in a wall, this lifting part lifts the body to the height of the hole. The form of the lift part is determined by the height h_1 and the width r_1 . Its form is shown in Fig. 12. There are two segment configurations depending on the height h_1 . In the case that $h_1 \leq 2r_1$, configuration A comprises two arc segments. In the case that $h_1 > 2r_1$, configuration B comprises two arc segments and one straight line segment. The center angle β_l of the arc of each configuration and the length d_l of the straight-line

Motions of snake robot



↔ Transitional by switching the role of the first unit

→ Transitional across different environments while meeting BC1 and BC2

↔ Transitional in the same env. by shift control

↔ Transitional in special case

Fig. 13. Transitional relationship between various motions.

segment in configuration B are given by

$$(\beta_l, d_l) = \begin{cases} \left(\arccos \left(1 - \frac{h_1}{2r_1} \right), 0 \right) & (h_1 \leq 2r_1) \\ \left(\frac{\pi}{2}, h_1 - 2r_1 \right) & (h_1 > 2r_1) \end{cases}. \quad (28)$$

The total length of the lift part l_{lift} is obtained as

$$l_{\text{lift}} = 2\beta_l r_1 + l_1. \quad (29)$$

D. Motion Transition

Transitable relationship between various motions is shown in Fig. 13. Each motion is classified according to whether it is TP-type or non-TP-type and the environment in which it can be applied.

The c-pedal wave is not a TP-type motion on its own, but by replacing the first unit with a shift part, the hoop-passing motion, which is TP-type, is performed. This motion transition is important in the change between TP and non-TP-type motion.

The red arrow in the figure indicates that transition across a different environments is possible. TP-type motions satisfy both BC1 and BC2 and transition between is possible across different environment.

The blue arrows in the figure indicate that transition in a given environment is possible (this must be distinguished from transition across different environments). For example, the c-pedal wave is designed so that the direction of movement due

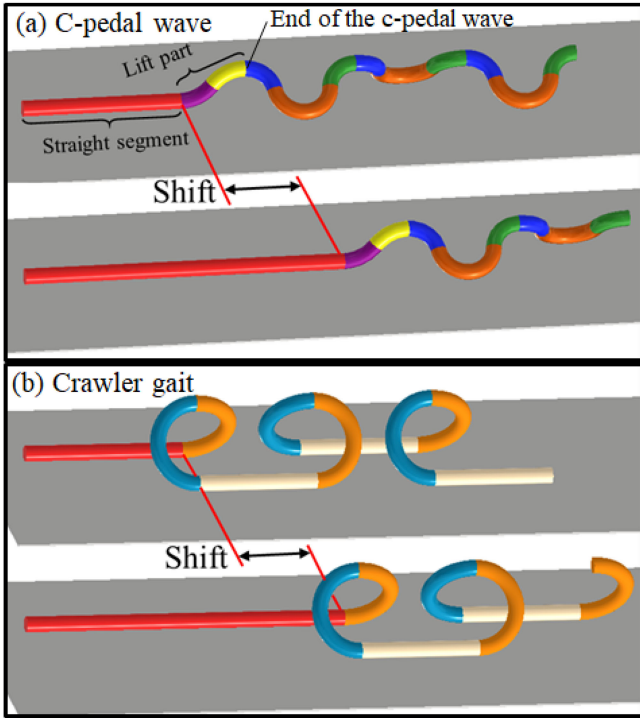


Fig. 14. Deformation to a straight form from (a) c-pedal wave and (b) crawler gait via shift control.

to shift control and the tangential directions of the two ends of the unit are parallel to one another. Therefore, as shown in the upper part of Fig. 14, by connecting the lift part and a straight segment beyond it, it is possible for the robot to deform into a straight form without slipping against the environment through shift control. Similarly, forms that can be deformed into the straight form can transition between one another through the straight form. The crawler gait, proposed in [31], also has a form in which the direction of propulsion due to shift control and the straight segments are parallel to one another, and the gait can be transformed into the straight form as shown at the bottom of Fig. 14. Therefore, the c-pedal wave and crawler gait can transition between one another through the straight form. Sidewinding [36] and helical rolling [27], [30] are also considered to be deformable to the straight form.

The green arrow indicates that helical rolling can be used for movement across different environments in a special case. Helical rolling is mainly used for movement inside or outside a pipe. It can also be used for movement on a flat surface. Therefore, it is possible to move from a pipe environment to a flat surface if the pipe outlet is located along the floor. Note that this transition does not satisfy BC1 and BC2. Although these transitions are different from that mainly considered in this article, we include them in Fig. 13 to show the diversity and potential of motion transitions.

The snake robot can transition from various type of motion to a c-pedal wave via the straight form on a plane and then transition to other TP-type motions through the hoop-passing motion. Transitions between diverse motions are, thus, possible via the hoop-passing motion.

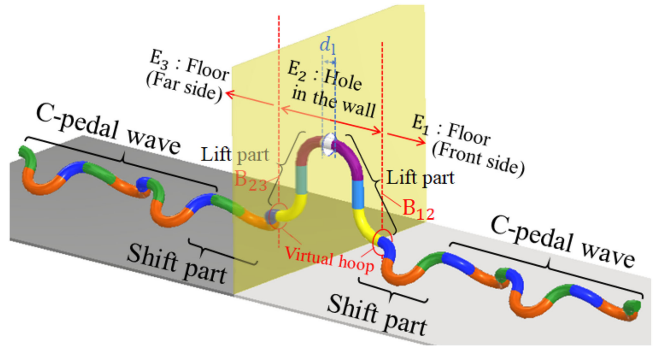


Fig. 15. Target form of passing through a hole in a wall.

VI. APPLICATION

A. Passing Through a Hole in a Wall

The hoop-passing motion is applied to design a motion passing through a hole in a wall. In this case, a snake robot should move across different environments twice, from the floor(E₁) to the hole in the wall(E₂) and from the hole in the wall(E₂) to the floor(E₃). An overview of the target form is shown in Fig. 15, and the process of motion transition is shown in Table V. In this motion, two form sets with connected c-pedal waves and shift parts are placed in front of and behind the wall, and they are connected by two lift parts. The two lift parts, which are parameterized according to the height of the hole, are connected by a straight segment corresponding to the part that passes through the wall. Let the length of this straight segment be d₁. The combination of the two lift parts and the straight segment is the form for the motion passing through the hole, and this part is a TP-type motion.

During the process, the shift part on the front side of the wall progresses through the hoop-passing motion as the body is pushed out to the hole side. In contrast, the shift part on the far side of the wall proceeds in the opposite direction to the front side of the hoop-passing motion as the body is pulled through the hole. For this reason, the shift parts on the front side and far side are always in the same phase, but when one phase progress is q, the other progress is set as 1 - q so as to generate an inverse transition.

B. Entering the Underfloor

We apply the hoop-passing motion to design a motion to pass through a hole in the floor and enter the underfloor. In this motion, the robot moves between different environments twice as in Section VI-A. An overview of the target form is shown in Fig. 16 while the process of motion transition is given in Table V. The basis of this behavior is the same as the motion described in Section VI-A. However, only one lift part is the form for passing through the hole and used to bridge the height difference between the groundfloor and underfloor. As an application, we consider changing the orientation of the c-pedal wave before and after the passage of the hole by ψ_{rot} . To this end, we suppose configuration B in Fig. 12, where the parameters of the lift part

TABLE V
MOTION TRANSITION PROCESS OF PASSING THROUGH A HOLE IN A WALL AND ENTERING THE UNDERFLOOR

E_1 : Floor	NB_{1-2}	NB_{2-1}	E_2 : Hole in the wall	NB_{2-3}	E_3 : Floor(Underfloor)	NB_{3-2}
M_1	CM_{1-2}	CM_{2-1}	M_2	CM_{2-3}	M_3	
c-pedal wave (Non-TP)	hoop passing motion (TP)	-	passing through a hole (TP)	-	hoop passing motion (TP)	c-pedal wave (Non-TP)

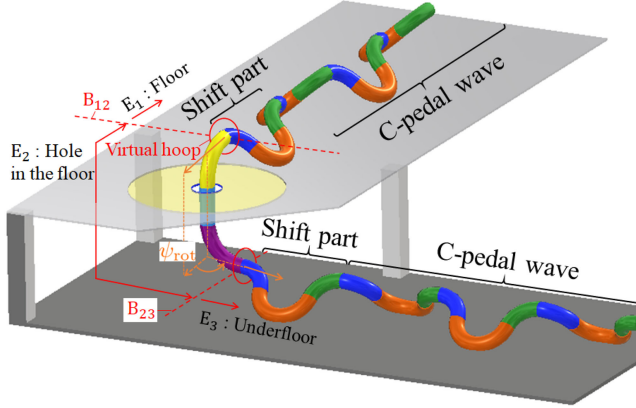


Fig. 16. Target form of entering the underfloor.

TABLE VI
MOTION TRANSITION OF ATTACHING TO A LADDER

E_1 : Floor	NB_{1-2}	NB_{2-1}	E_2 : Ladder
M_1	CM_{1-2}	CM_{2-1}	M_2
crawler gait (Non-TP)	straight form → c-pedal wave(Non-TP) → hoop passing motion(TP)	-	ladder climbing (TP)

are $h_l > 2r_l$, and set the torsion angle between the second and third segments of the lift part ψ_{rot} . Let h_1 equal the difference in height between the surface of the groundfloor and underfloor.

C. Attaching to a Ladder

As an example of the application of hoop-passing motion, the motion of attaching to a ladder from a floor is designed. The motion used in climbing a ladder [32] is classified as being of TP-type. As an example, by combining the deformations shown in Fig. 14 and the hoop-passing motion, the snake robot can move over rough terrain with the crawler gait and transform into the c-pedal wave via the straight form, and then attach to the ladder adopting the hoop-passing motion, as shown in Table VI. The arrows in Table VI show the motion transition in the same area.

1) *Gait Design for Ladder Climbing:* First, we briefly describe the target form for the ladder climbing proposed in [32].

The basic form of the gait required to climb a ladder is shown in Fig. 17. This form consists of repeatedly connected units that are configured by combining six simple shapes. One unit corresponds to one step of the ladder. The shapes of the segments are defined using h_s , l_s , α , and r_c , as shown in Table VII, where $n \in \mathbb{N}$ is a unit index. h_s and l_s are, respectively, the vertical interval and horizontal interval between the steps of the ladder. These intervals are dependent on the shape of the ladder. α is the angle shown in Fig. 17. Increasing α increases the height of

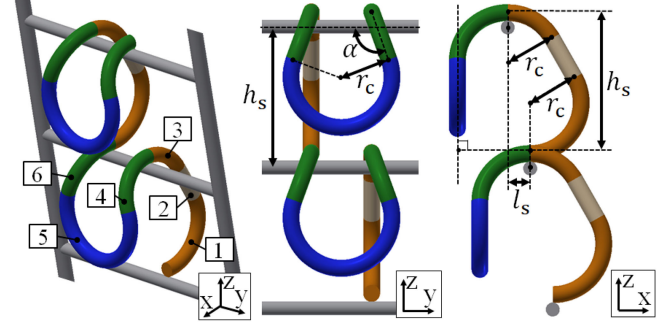


Fig. 17. Segment configuration for the ladder climbing motion [32].

TABLE VII
PARAMETERS OF SEGMENTS USED TO COMPOSE THE GAIT REQUIRED TO CLIMB A LADDER [32]

seg no. j	type	parameter	$\hat{\psi}_j$
$6n + 1$	circular arc	$(r_j, \phi_j) = (r_c, \frac{\pi}{2} + \beta)$	$(-1)^n(\alpha + \frac{\pi}{2})$
$6n + 2$	straight line	$l_j = (h_s - 2r_c)/\cos \beta$	0
$6n + 3$	circular arc	$(r_j, \phi_j) = (r_c, \frac{\pi}{2} - \beta)$	0
$6n + 4$	circular arc	$(r_j, \phi_j) = (r_c, \frac{\pi}{2})$	$(-1)^n(\alpha - \frac{\pi}{2})$
$6n + 5$	circular arc	$(r_j, \phi_j) = (r_c, 2\alpha)$	$(-1)^{n+1}\frac{\pi}{2}$
$6n + 6$	circular arc	$(r_j, \phi_j) = (r_c, \frac{\pi}{2})$	$(-1)^n\frac{\pi}{2}$

the far side of the ladder to make it easier for the snake robot to grab the step but also increases the required length of the snake robot per step on the ladder. r_c is the radius of all circular arcs. A smaller value of r_c means that the required length of the snake robot per step is shorter, while a larger r_c value makes the robot form smoother. The minimum value of r_c is determined from the shape constraints while considering θ_{\max} , as discussed in [31]. β in Table VII can be obtained according to the geometrical relationship as

$$\beta = \arctan \left(\frac{l_s}{h_s - 2r_c} \right). \quad (30)$$

Therefore, to be able to calculate β , h_s must meet the condition

$$h_s > 2r_c. \quad (31)$$

Shift control is used to generate the ladder climbing motion. It is possible to climb up the ladder by shifting s_h in the positive direction and to climb down the ladder by shifting s_h in the negative direction.

2) *Connecting to the Hoop-Passing Motion:* We explain how to apply the hoop-passing motion to ladder climbing. In this motion, the next form is the form connecting the form of the ladder climbing described in Section VI-C1 and the lift part. In other words, form-1 is the c-pedal wave, form-2 is a lift part, form-3 is a lift part, and form-4 explained in Section V-A is the ladder climbing action. The lift part is connected to the position



Fig. 18. Snake robot [32].

of the connecting part-3 among the target forms of the ladder climbing motion. So that the tip of the lift part rides exactly on the first step of the ladder, h_l is determined as

$$h_l = h_s - h_p. \quad (32)$$

We formulate the configuration of the next form. The lengths of form-3 and form-4 and the starting point for connecting each form are given as

$$l_{f3} = \begin{cases} l_t & (l_t \leq l_{lift}) \\ l_{lift} & (l_{lift} < l_t) \end{cases} \quad (33)$$

$$l_{f4} = \begin{cases} 0 & (l_t \leq l_{lift}) \\ l_t - l_{lift} & (l_{lift} < l_t) \end{cases} \quad (34)$$

$$s_{f3} = 0 \quad (35)$$

$$s_{f4} = \pi r_c + \frac{h_{sn} - 2r_c}{\cos \beta_n}. \quad (36)$$

On the abovementioned basis, we first perform motion transitions using hoop passing motions as $s_h = l_{robot}$. When a sufficient length of the snake robot body can be transitioned to the ladder climbing form, the climbing of the ladder can be performed by shift control.

VII. EXPERIMENT

A. Design of a Snake Robot

We here describe the development of a snake robot with a smooth surface shape proposed in [32]. In this article, we conducted experiments using this robot.

The system configuration of the snake robot is shown in Fig. 18. The snake robot has a module configuration in which each module comprises a link and joint, as shown in Fig. 19. The link length l is 70 mm, the diameter of the thickest part of the link is 56 mm, and the mass of a single module is approximately 0.15 kg. All joints have a range of motion of 180 deg.; i.e., $\theta_{max} = 90$ deg. A DYNAMIXEL XH430-V350-R (ROBOTIS) is used as the joint actuator and the maximum torque is approximately 4.0 Nm. The robot has 36 joints. The snake robot is powered via a power cable and the target angle for each joint is sent from a computer on the operator side through an RS485

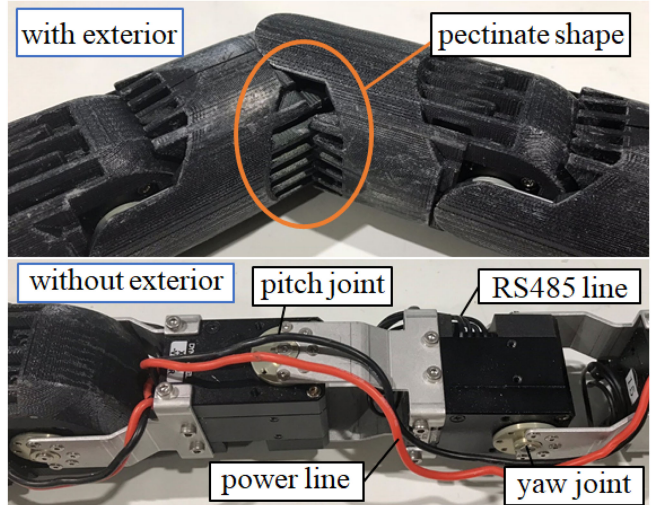


Fig. 19. Module Configuration [32].

interface. It is possible to obtain information about the robot, including the joint angle and motor current. The sampling time required to update the target joint angle is 20 ms. The operator can control the robot's operations via a gamepad. According to [31], the maximum curvature κ_{max} that can be achieved by this snake robot is 0.0112 mm⁻¹. The minimum value of the radius r_{min} is, thus, 89.1 mm.

To ensure that the snake robot can move without becoming stuck in the environment, it is important that its exterior body surface is smooth. We, therefore, developed a snake robot that had a smooth exterior body surface by giving the links the pectinate shape shown at the top of Fig. 19. In this design, the surface shape is smoothed using the pectinate part, and this part does not affect the bending of joints. The interval between the teeth of the comb structure is 3 mm, which means that debris larger than 3 mm does not get inside the robot.

B. Parameters of the C-Pedal Wave

Three experiments were conducted to verify the effectiveness of the proposed method. The first experiment was conducted for motion through a hole in a wall, the second for motion through a hole in the floor and entering the underfloor, and the third for attaching to a ladder after moving along a floor. The form parameters of the c-pedal wave and the shift part common to all experiments were set as $h_p = 100$ mm, $w_p = 250$ mm, $d_p = 400$ mm, and $\epsilon_s = 10$ mm.

C. Passing Through a Hole in a Wall

We conducted an experiment for a snake robot passing through a hole in a wall. An acrylic plate having thickness of 5 mm and a hole with a diameter of 80 mm was placed vertically. The center of the hole was located at a height of 500 mm from the floor. The parameters of the lift part were $h_l = 372$ mm and $r_l = 100$ mm, and the length of the straight line through the hole part was $d_l = 50$ mm.

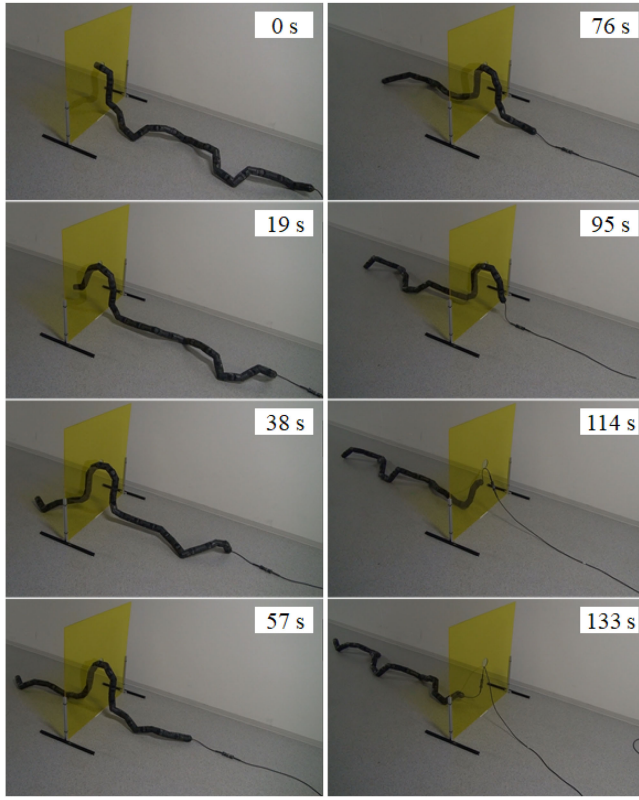


Fig. 20. Results of the experiment of passing through a hole in a wall.

The experimental results are shown in Fig. 20 and the video “Extension1-passing-through-the-hole-in-the-wall.mp4”. We started the experiment with the head placed on the edge of the hole in the wall due to the difficulty in maintaining fine enough control and lack of torque to support a long link of snake, the experiment started with the head of the snake robot placed in the hole in the wall. It was able to pass the snake robot through the hole by performing the hoop-passing motion. The smooth surface shape of the robot allowed the robot to pass through the hole without being caught on the edge of the hole.

If the curvature of the target form around the hole is large, the joint angle of the snake robot there becomes large, and the robot was sometimes unable to pass through the hole because it was caught around the hole. Therefore, in making the robot form near the hole, r_1 was set larger than the minimum value $r_{\min} = 89.1$ mm determined by the joint range limitation [31] while d_1 was set larger than the thickness of the wall.

D. Entering the Underfloor

The experiment was conducted for the snake robot passing through a hole in the floor, assuming an application of inspection under the floor. Acrylic plates with a thickness of 5 mm were fixed horizontally to prepare a floor surface with a height of 335 mm. The hole was 80 mm in diameter. The parameters of the lift part were set to $h_l = 335$ mm and $r_1 = 100$ mm. Assuming that the direction of travel must change after the robot enters the subfloor, we set $\psi_{\text{rot}} = 90$ deg.

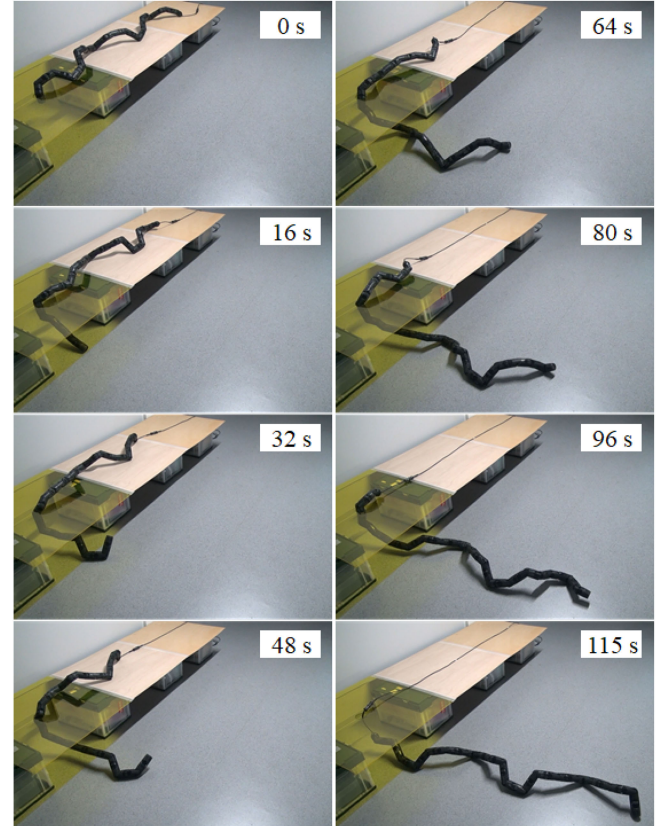


Fig. 21. Result of the experiment of entering the underfloor.

The experiment is shown in Fig. 21 and the video “Extension2-entering-under-the-floor.mp4”. The head of the snake robot was placed at the end of the first segment of the target form of the lift part, and the experiment began with the head inserted into the hole. The hoop-passing motion allowed the snake robot to pass through a hole in the floor and enter the underfloor while changing its orientation by 90 deg.

E. Attaching to the Ladder

In a previous study [32], we conducted an experiment in which the snake robot attached itself to a ladder while transitioning to a (TP-type) ladder climbing gait after moving across the floor with a crawler gait (non-TP-type), via the (non-TP-type) c-pedal wave [31]. The crawler gait allows the robot to move at high speed even on uneven terrain and to turn and adjust its position finely. In this experiment, both motions of approaching and attaching to the ladder were considered. Assuming the shape of the ladder is known, we let $h_{sn} = 150$ mm, $l_{sn} = 0$ mm, and $r_c = r_{\min}$. Additionally, the parameters of the lift part were $h_l = 210$ mm and $r_1 = r_{\min} = 89.1$ mm.

The process of the experiment is described below.

- Step 1:* The snake robot moved across the floor and approached the ladder adopting the crawler gait (Non-TP Type).
- Step 2:* Step 2 The arc segment of the crawler gait was deformed and the head of the snake robot was hung on the first step of the ladder. The form of this hanging part

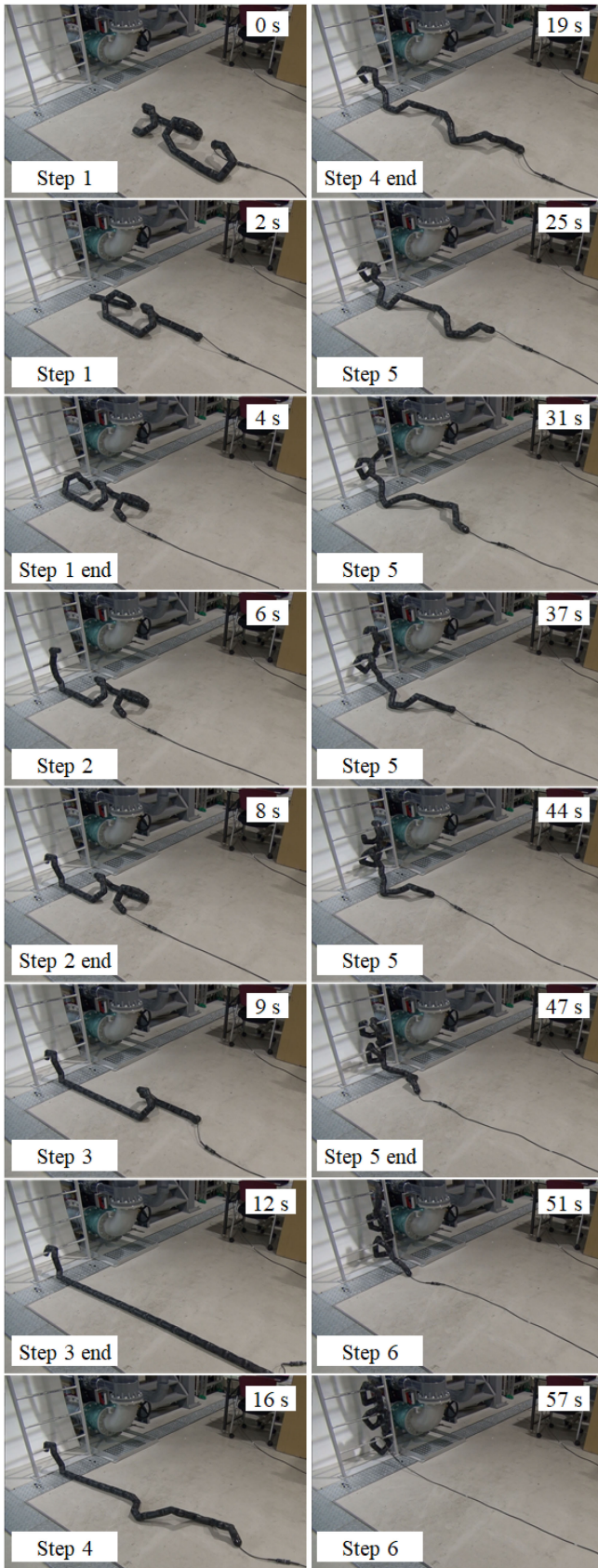


Fig. 22. Results of the experiment of attaching to the ladder.

was designed in advance by combining straight lines and arcs.

- Step 3:* Step 3 The form of the crawler gait was shifted to the tail side and became a straight form.
- Step 4:* Step 4 The straight form was deformed to the (non-TP-type) c-pedal wave form through shift control from the tail side to the head side.
- Step 5:* Step 5 The first unit of the c-pedal wave was replaced with a shift part and attached to the ladder by performing the hoop-passing motion (as CM₁₋₂).
- Step 6:* Step 6 The robot climbed the ladder (TP-type motion) through shift control.

In this process, the set of motions of transforming to the straight form, the c-pedal wave, and the hoop-passing motion are regarded as CM₁₋₂, as shown in Table VI. We advanced from Step 5 to Step 6 when the length of the tail side before the lift part became less than 600 mm, terminated the hoop-passing motion, and transitioned to ladder climbing through simple shift control. The experimental results are shown in Fig. 22 and the video “Extension3-attaching-to-the-ladder.mp4”. Using the proposed hoop-passing motion, the snake robot climbed the ladder after moving across the floor with the crawler gait.

VIII. CONCLUSION

In this article, we worked on solving the problem of transitioning the motion of a snake robot across different environments to expand the application environment of the snake robot. We first found that it is important that the motion at the connection point between the two motions coincides with the tangential movement when performing such a transition and satisfying boundary conditions BC1 and BC2. Additionally, we classified the motions of the snake robot into two types: the TP-type, in which the body moves in a tangential direction using the lateral constraint of a passive wheel or obstacle, and the non-TP-type. Such a transition is easy if it is between TP-type motions. Meanwhile non-TP-type motions are not suitable for transition across different environments, but non-TP-types include important motions such as those that do not require slippage between the snake robot body and the environment.

We then designed a special gait called the circular pedal wave (c-pedal wave), which does not require sliding but at the same time allows TP-type motion. The c-pedal wave combined with deformation of the shift part allows a TP-type “hoop-passing motion” in which the whole body moves as if it were passing through a virtual hoop fixed in space in sequence from its head. Furthermore, some non-TP-type motions can transform to the c-pedal wave via the straight form in the same environment. Consequently, it is possible to transform the motion across a discontinuous environment change even if the process includes a non-TP-type motion. We conducted experiments to verify the effectiveness of our proposed method. In the first experiment, the passage of a snake robot through a hole in a vertical wall was achieved. In the second experiment, we propelled the robot through a hole in the floor and into the underfloor while changing

the direction of propulsion. In the third experiment, after moving across the floor with the crawler gait, the robot placed its head by itself and deformed to the c-pedal wave via the straight form. Afterward, the robot successfully executed motion transition and climbed the ladder.

Finally, future works are discussed. In this article, we focused only on the transition between TP-type motions in which the connection point between two motions moves only in the tangential direction of the trunk. The motions of the snake robot are complicated because of not only the change in body form curve but also the combination of rolling motions. The crawler gait, sidewinding, helical rolling, and c-pedal wave are capable of transitioning to one another via the straight form, there are likely to be a variety of other ways to transition between motions. The generalization of the method for transforming a variety of gait forms into the straight form in various environments is an issue that needs to be addressed in future work. Furthermore, in the proposed method, the hoop-passing motion is restricted to a two-dimensional plane. When the hoop-passing motion is performed on uneven terrain, the tip of the shift part cannot be fixed to the environment during the movement of the c-pedal wave. A possible solution to this problem is to add a part next to the shift part to counteract the motion of the latter part and, thus, stabilize the robot; however, this requires a large joint torque to lift the long robot body. This problem will be considered in future work.

Regarding the experiments described in Sections VII-C and VII-D, a future challenge will be to realize the ability of the snake to insert its head into the hole. While in theory, it would be possible for the robot to approach the wall and place its head in the hole independently. The c-pedal wave could be moved back and forth via shift control and left and right via rolling, but the system lacks control fidelity to do so effectively, particularly as the snake is not capable of yawing. Furthermore, lifting the head sufficiently high would require greater torque than can be produced by the servos.

Future work will seek to improve control fidelity and find motions that minimize torque requirements. One approach to solve this problem is to design the target form of the snake robot in such a way that the moment on the body is reduced considering the density of the robot. Another is to optimize the parameters of the proposed forms (i.e., h_p , w_p , and d_p for the c-pedal wave). In addition, in some cases, the snake robot has few grounding points and thus becomes unstable during transition. One solution to this problem is to increase the number of joints and the body length of the snake robot to create more grounding points. Another solution is to shorten the interval of the units of the c-pedal wave to increase the number of grounding points; however, this method is difficult to achieve because of the limited joint motion range.

REFERENCES

- [1] S. Hirose, *Biologically Inspired Robots: Snake-Like Locomotor and Manipulator*, Oxford, U.K.: Oxford Univ. Press, 1987.
- [2] M. Saito, M. Fukaya, and T. Iwasaki, "Serpentine locomotion with robotic snakes," *IEEE Control Syst.*, vol. 22, no. 1, pp. 64–81, Feb. 2002.
- [3] P. Liljeback, I. U. Haugstuen, and K. Y. Pettersen, "Path following control of planar snake robots using a cascaded approach," *IEEE Trans. Control Syst. Technol.*, vol. 20, no. 1, pp. 111–126, Jan. 2012.
- [4] A. Mohammadi, E. Rezapour, M. Maggiore, and K. Y. Pettersen, "Maneuvering control of planar snake robots using virtual holonomic constraints," *IEEE Trans. Control Syst. Technol.*, vol. 24, no. 3, pp. 884–899, May 2016.
- [5] P. Prautsch, T. Mita, and T. Iwasaki, "Analysis and control of a gait of snake robot," *Trans. Electr. Electron. J.*, vol. 120-D, pp. 372–381, 2000.
- [6] K. Watanabe, M. Iwase, S. Hatakeyama, and T. Maruyama, "Control strategy for a snake-like robot based on constraint force and verification by experiment," *Adv. Robot.*, no. 23, pp. 907–937, 2009.
- [7] F. Matsuno and K. Mogi, "Redundancy controllable system and control of snake robot based on kinematic model," in *Proc. IEEE Conf. Decis. Control*, 2000, pp. 4791–4796.
- [8] F. Matsuno and H. Sato, "Trajectory tracking control of snake robots based on dynamic model," in *Proc. IEEE Int. Conf. Robot. Autom.*, 2005, pp. 3040–3046.
- [9] M. Tanaka and F. Matsuno, "Modeling and control of head raising snake robots by using kinematic redundancy," *J. Intell. Robot. Syst.*, vol. 75, no. 1, pp. 53–69, 2014.
- [10] M. Ishikawa, K. Owaki, M. Shinagawa, and T. Sugie, "Control of snake-like robot based on nonlinear controllability analysis," in *Proc. IEEE Int. Conf. Control Appl.*, 2010, pp. 1134–1139.
- [11] M. Tanaka and K. Tanaka, "Control of a snake robot for ascending and descending steps," *IEEE Trans. Robot.*, vol. 31, no. 2, pp. 511–520, Apr. 2015.
- [12] A. A. Transeth, R. I. Leine, C. Glocker, K. Y. Pettersen, and P. Liljeback, "Snake robot obstacle-aided locomotion: Modeling, simulations, and experiments," *IEEE Trans. Robot.*, vol. 24, no. 1, pp. 88–104, Feb. 2008.
- [13] P. Liljeback, K. Y. Pettersen, Ø. Stavdahl, and J. Tommy Gravdahl, "Compliant control of the body shape of snake robots," in *Proc. IEEE Int. Conf. Robot. Autom.*, 2014, pp. 4548–4555.
- [14] T. Kamegawa, T. Watanabe, S. Yuan, and A. Gofuku, "Reactive motion for a snake-like robot in a crowded space," *Nucl. Saf. Simul.*, vol. 6, no. 2, pp. 109–115, 2015.
- [15] T. Kano, R. Yoshizawa, and A. Ishiguro, "TEGOTAE-based control scheme for snake-like robots that enables scaffold-based locomotion," in *Proc. 5th Int. Conf. Biomimetic Biohybrid Syst.*, 2016, pp. 454–458.
- [16] M. Tesch *et al.*, "Parameterized and scripted gaits for modular snake robots," *Adv. Robot.*, vol. 23, no. 9, pp. 1131–1158, 2009.
- [17] M. Yin and S. Homans, and K. Roufas, "Climbing with snake-like robots," in *Proc. IFAC Workshop Mobile Robot Technol.*, 2001, pp. 7–12.
- [18] D. Rollinson and H. Choset, "Pipe network locomotion with a snake robot," *J. Field Robot.*, vol. 33, no. 3, pp. 322–336, 2016.
- [19] M. Travers, J. Whitman, and H. Choset, "Shape-based coordination in locomotion control," *Int. J. Robot. Res.*, vol. 37, no. 10, pp. 1253–1268, 2018.
- [20] G. S. Chirikjian and J. W. Burdick, "The kinematics of hyper-redundant robot locomotion," *IEEE Trans. Robot. Autom.*, vol. 11, no. 6, pp. 781–793, Dec. 1995.
- [21] S. B. Andersson, "Discretization of a continuous curve," *IEEE Trans. Robot.*, vol. 24, no. 2, pp. 456–461, Apr. 2008.
- [22] R. L. Hatton and H. Choset, "Generating gaits for snake robots: Annealed chain fitting and keyframe wave extraction," *Auton. Robot.*, vol. 28, no. 3, pp. 271–281, 2010.
- [23] P. Liljeback, K. Y. Pettersen, Ø. Stavdahl, and J. T. Gravdahl, "A 3D motion planning framework for snake robots," in *Proc. IEEE/RSJ Int. Conf. Intell. Robots Syst.* 2014, pp. 1100–1107.
- [24] H. Yamada and S. Hirose, "Study of active cord mechanism - approximations to continuous curves of a multi-joint body," *J. Robot. Soc. Jpn.*, vol. 26, no. 1, pp. 110–120, 2008. (in Japanese with English Summary)
- [25] H. Yamada and S. Hirose, "Study on the 3D shape of active cord mechanism," in *Proc. IEEE Int. Conf. Robot. Automat.*, 2006, pp. 2890–2895.
- [26] H. Yamada, S. Takaoka, and S. Hirose, "A snake-like robot for real-world inspection applications (the design and control of a practical active cord mechanism)," *Adv. Robot.*, vol. 27, no. 1, pp. 47–60, 2013.
- [27] T. Kamegawa, T. Harada, and A. Gofuku, "Realization of cylinder climbing locomotion with helical form by a snake robot with passive wheels," in *Proc. IEEE Int. Conf. Robot. Automat.*, 2009, pp. 3067–3072.
- [28] T. Baba, Y. Kameyama, T. Kamegawa, and A. Gofuku, "A snake robot propelling inside of a pipe with helical rolling motion," in *Proc. SICE Annu. Conf.*, 2010, pp. 2319–2325.
- [29] T. Kamegawa, T. Baba, and A. Gofuku, "V-shift control for snake robot moving the inside of a pipe with helical rolling motion," in *Proc. IEEE Int. Symp. Safety, Security, Rescue Robot.*, 2011, pp. 1–6.

- [30] W. Zhen, C. Gong, and H. Choset, "Modeling rolling gaits of a snake robot," in *Proc. IEEE Int. Conf. Robot. Automat.*, 2015, pp. 3741–3746.
- [31] T. Takemori, M. Tanaka, and F. Matsuno, "Gait design for a snake robot by connecting curve segments and experimental demonstration," *IEEE Trans. Robot.*, vol. 34, no. 5, pp. 1384–1391, Oct. 2018.
- [32] T. Takemori, M. Tanaka, and F. Matsuno, "Ladder climbing with a snake robot," in *Proc. IEEE/RSJ Int. Conf. Intell. Robots Syst.*, 2018, pp. 8140–8145.
- [33] Q. Fu and C. Li, "Robotic modelling of snake traversing large, smooth obstacles reveals stability benefits of body compliance," *Roy. Soc. Open Sci.*, vol. 7, no. 2, 2020.
- [34] M. Nakajima, M. Tanaka, K. Tanaka, and F. Matsuno, "Motion control of a snake robot moving between two non-parallel planes," *Adv. Robot.*, vol. 32, no. 10, pp. 559–573, 2018.
- [35] T. Kano, R. Yoshizawa, and A. Ishiguro, "Tegotae-based decentralised control scheme for autonomous gait transition of snake-like robots," *Bioinspiration Biomimetics*, vol. 12, no. 4, pp. 1–20, 2017.
- [36] J. W. Burdick, J. Radford, G. S. Chirikjian, "A 'sidewinding' locomotion gait for hyper-redundant robots," in *Proc. IEEE Int. Conf. Robot. Automat.*, 1993, pp. 101–106.
- [37] H. Ohno and S. Hirose, "Design of slim slime robot and its gait of locomotion," in *Proc. IEEE/RSJ Int. Conf. Intell. Robots Syst.*, 2001, pp. 707–715.



Tatsuya Takemori (Student Member, IEEE) received the B.S. and M.S. degrees in engineering in 2016 and 2018, respectively, from the Department of Mechanical Engineering and Science, Kyoto University, Kyoto, Japan, where he is currently working toward the Ph.D. degree with the Department of Mechanical Engineering and Science, Graduate School of Engineering.

His research interests include biologically inspired robotics, entertainment computing, and rescue support systems in fires and disasters.

Mr. Takemori was the recipient of the Japan Society of Mechanical Engineers Award, in 2019, and the Institute of Systems Control and Information Engineers Young Researcher Award in 2020.



Motoyasu Tanaka (Member, IEEE) received the B.S., M.S., and Ph.D. degrees in engineering from the Department of Mechanical Engineering and Intelligent Systems, The University of Electro-Communications, Tokyo, Japan, in 2005, 2007, and 2009, respectively.

From 2009 to 2012, he was with the Canon, Inc., Tokyo, Japan. He is currently a Professor with the Department of Mechanical and Intelligent Systems Engineering, University of Electro-Communications. His research interests include biologically inspired robotics and dynamic-based nonlinear control.

Prof. Tanaka was the recipient of the IEEE Robotics and Automation Society Japan Chapter Young Award from the IEEE Robotics and Automation Society Japan Chapter in 2006, and the Best Poster Award at SWARM2015: The First International Symposium on Swarm Behavior and Bio-Inspired Robotics, Kyoto, Japan, in 2015.



Fumitoshi Matsuno (Member, IEEE) received the Dr.Eng. degree from Osaka University, Suita, Japan, in 1986.

In 1986, he was with the Department of Control Engineering, Osaka University. Since 2009, he has been a Professor with the Department of Mechanical Engineering and Science, Kyoto University. He is the Vice President of the Robotics Society of Japan and the NPO International Rescue System Institute, and was the President of the Institute of Systems, Control, and Information Engineers. His research interests include robotics, swarm intelligence, and control of nonlinear and distributed parameter systems.

Prof. Matsuno was the recipient of the Best Paper Awards in 2001, 2006, and 2017 from the Society of Instrument and Control Engineers (SICE), in 2013 from the Information Processing Society of Japan, and in 2018 from the RSJ, and the Prize for Academic Achievement from the Japan Society of Mechanical Engineers in 2009. He is the General Chair of DARS-SWARM2021 and ASCC2022, and was the General Chair of IEEE SSRR2011, IEEE/SICE SII2011, SWARM2015, SWARM2017, etc. He is a Fellow Member of the SICE, JSME, and RSJ.